Available online at www.sciencedirect.com
ScienceDirect
Journal of Computational Physics 226 (2007) 2044–2062
JOURNAL OF COMPUTATIONAL PHYSICS
www.elsevier.com/locate/jcp

Octant flux splitting information preservation DSMC method for thermally driven flows

Nathan D. Masters [a], Wenjing Ye [b,c,*]

[a] University of California, Lawrence Livermore National Laboratory, USA
[b] Woodruff School of Mechanical Engineering, Georgia Institute of Technology, USA
[c] Department of Mechanical Engineering, Hong Kong University of Science and Technology, Clear Water Bay, Kawloon, Hong Kong

Received 6 February 2007; accepted 26 June 2007
Available online 6 July 2007

Abstract

We present the octant flux splitting DSMC method as an efficient method for simulating non-equilibrium flows of rarefied gas, particularly those arising from thermal loading. We discuss the current state-of-the-art flux splitting IP-DSMC technique and show that it fails to capture the shear stresses created by thermal gradients. We present the development of the octant flux splitting IP-DSMC as well as degenerate 2D, 1D, and 0D forms and apply the method to a number of problems including thermal transpiration, with satisfactory results.

Keywords: Rarefied gas; Thermally driven flow; Thermal transpiration; DSMC; Information preserving methods

1. Introduction

A number of interesting phenomena may occur in the presence of thermal loading in a rarefied gas. In 1825, Fresnel noticed that small bodies suspended in a gas would sometimes move when exposed to light—something later studied in detail by Crookes and others using a variety of the now familiar radiometers [1]. In 1879, Osborne Reynolds gave the name thermal transpiration to the effect he observed wherein gas was pumped through capillaries or porous plugs subject to a temperature gradient. In that same year, James Clerk Maxwell proposed a theoretical explanation for the mechanism of both thermal transpiration and the radiometric effect [2]. Recently, a number of micro- and nanoscale systems have sought to leverage thermally driven rarefied gas dynamic phenomena for pumping [3–6], propulsion [7] and sensing [8]. Although the physical mechanisms are understood, detailed modeling of such systems is complicated by the difficulty involved in modeling low-speed non-equilibrium rarefied gas systems.

* Corresponding author. Address: Department of Mechanical Engineering, Hong Kong University of Science and Technology, Clear Water Bay, Kawloon, Hong Kong. Tel.: +852 2358 7194; fax: +852 2358 1543.
E-mail address: mewye@ust.hk (W. Ye).

0021-9991/$ - see front matter
doi:10.1016/j.jcp.2007.06.027

The degree of rarefaction of a gas is quantified by the Knudsen number which is the ratio of the mean free path between intermolecular collisions (λ) and some characteristic length, L, of the flow; i.e., $Kn = \lambda/L$. At small Kn, the intermolecular collisions dominate – resulting in a diffusive nature that can be accurately described by continuum models, e.g., the Euler and Navier–Stokes equations [9,10]. At larger Kn, either due to decreasing densities (and correspondingly larger mean free paths) or smaller characteristic lengths, the contribution of intermolecular collisions will diminish until conservation equations cease to form a closed set at $Kn > 0.1$ and the continuum description breaks down [9]. Within the *transition* regime, $0.1 < Kn < 10$, intermolecular collisions remain important – but not dominant – and the molecular nature of the gas must be considered. Finally, the free molecular regime, $Kn > 10$, is characterized by extremely rare intermolecular collisions and ballistic transport.

The fundamental equation describing the molecular nature of gases is the Boltzmann transport equation (BTE). One method of solving the BTE is a direct mathematical approach using distribution functions as the primary variables. However, the solution of the complete BTE has proven very difficult, requiring significant computational expense evaluating distributions and collision integrals. This has led to the development of various linearized models and simplified collision integrals (BGK, S-model, etc.) suitable for a range of slightly non-equilibrium problems [11]. An alternative approach is to model the behavior of the individual molecules directly, leading to a molecular dynamics (MD) approach. However, the large number of molecules (and the associated computational expense) required to adequately model a dilute gas precludes the MD approach. The direct simulation Monte Carlo largely overcomes this difficulty by using simulation molecules, each representing a large number of real molecules. This has the additional advantage that collisions—partners and post-collision behavior—may be treated in a probabilistic sense for further computational efficiency [9].

Although the DSMC has been used to model a number of thermally driven problems, including transpiration [6], such problems typically require a large number of samples. Low-speed flows, common in both small-scale devices and thermally driven systems, pose a particular challenge to efficient DSMC simulation as a large number of samples are required to control statistical noise. For example, air at standard temperature and pressure (STP) is composed of a myriad of molecules, each with velocities on the order of 500 m/s which are essentially independent of the stream velocity. A DSMC simulation of a 1 m/s flow of air at STP would require over 8×10^6 independent samples to resolve the stream velocity within 1% [12].

The slow convergence of the DSMC simulations of low-speed flows has motivated the development of specialized DSMC techniques. Pan et al. proposed a DSMC method which split the molecular velocities into two parts: thermal and flow. By considering only the flow component in sampling they succeeded in reducing scatter for certain isothermal flows [13]. In a subsequent paper, Pan et al. [14] developed a block model suitable for non-isothermal flows wherein "big molecules" with modified masses and collision cross sections are used to replace the conventional simulation molecules. However, as pointed out in [30], the molecular block model doesn't preserve the same flow conditions and thus is not accurate. Chun and Koch recently proposed a heavily modified DSMC which adds "ghost" molecules and variable weighting of particles during collisions and sampling [15].

The obvious similarity in all of these methods is to separate the information due to thermal energy from that associated with the stream velocity. The information preserving DSMC (IP-DSMC), originally proposed by Fan and Shen, is another such method that achieves variance reduction by storing and propagating certain collective quantities (information) with each simulation molecule [16]. If we consider each simulation (DSMC) molecule to be a representative sample from a large set of real molecules (i.e., with a position and velocity that an individual real molecule could have), then the preserved (IP) quantities may be interpreted as approximations of the collective, or macroscopic, information of the ensemble of *real* molecules represented by the *simulation* particle. Within the simulation, preserved quantities are propagated by particle motion (DSMC velocity) and sampled to obtain the macroscopic averages for the ensemble of particles within the computational cells. The resulting samples reflect the reduced noise in the preserved quantities.

The initial IP-DSMC model presented by Fan and Shen preserved only the velocity, which proved adequate for the isothermal channel flow they considered [16]. Subsequently, the IP-DSMC has been extended to treat more general flows by preserving additional quantities—density and temperature—and by various models for the transport and conservation of mass, momentum, and energy [17–22]. In all cases, an update step accounts for the effects of mass, momentum and energy transport not captured by simulation particle movement. The early development of these IP-DSMC update techniques, as reported in the literature, has been somewhat ad

hoc, beginning with the intuitive formulation for the acceleration of the gas due to pressure gradients [18,23]. For non-isothermal flows, the transport of energy must be treated carefully and several methods have been proposed with varying degrees of success and applicability, including: modified collision cross-sections [18], the introduction of "additional energies" to molecules migrating between cells [20], and fluxal terms derived from kinetic theory [19,21]. Recently, Sun and Boyd derived update equations that provide a formal connection between the preserved quantities and Maxwell's equation of change and proposed two models to complete the update formulae, namely the local thermal equilibrium (LTE) and flux splitting (FS) methods [22]. To date, the flux splitting IP-DSMC technique appears to be the most accurate and generally applicable of the IP-DSMC techniques.

The performance and accuracy of the various IP-DSMC techniques has been demonstrated with satisfactory results through a number of benchmark problems including Poiseuille, Rayleigh, and thermal and velocity Couette flows, as well as shock structure problems in argon gas [20,22]. In this paper, we are interested in applying IP-DSMC techniques to low-speed thermally driven flows, e.g., thermal transpiration. In doing so, we will show that the current (flux splitting) IP-DSMC methods cannot adequately model such flows. We will present the development of an "Octant" flux splitting IP-DSMC (or OSIP-DSMC) technique for efficient modeling of low-speed non-equilibrium rarefied gas flows, especially those arising from thermal loading.

The balance of this paper is organized as follows: Section 2 a brief review of the current state-of-the-art IP-DSMC methods; Section 3 a description of thermal transpiration and IP-DSMC modeling. The failure of the flux splitting method leads to the development of the Octant Splitting IP-DSMC presented in Section 4. Section 5 reports on the results of benchmark problems as well a few example problems, including thermal transpiration in a microchannel and thermal cavity problems. Finally, we present our conclusions in Section 6.

2. Review of current IP-DSMC methods

In the DSMC, each simulation molecule represents a large number, F_N, of real molecules such that a set of M simulation molecules represents $M \cdot F_N$ real molecules. Each of these simulation molecules has a mass, m, corresponding to the molecular mass of the species being modeled and position, $\mathbf{x}$, and velocity, $\mathbf{c}$, consistent with the spatial location and microscopic velocities, $\boldsymbol{\xi}$, of the real molecules. The simulation molecules are then allowed to move within the computational domain: interacting with boundaries as appropriate and with other simulation molecules through a probabilistic treatment of collisions. Macroscopic quantities are obtained by averaging the microscopic velocities and densities of the simulation molecules. The IP-DSMC supplements the DSMC velocity and position with certain preserved quantities that represent the collective, or macroscopic, properties of some large set of "real" molecules that could be represented by the simulation molecule. Thus, the preserved velocity, $\mathbf{V}$, represents the average velocity of these "real" molecules, i.e., $\mathbf{V} = \overline{\boldsymbol{\xi}}$. The preserved temperature, T_{IP}, represents the energy associated with the thermal velocities of these "real" molecules relative to the preserved velocity, i.e., $T_{\mathrm{IP}} = (\overline{\xi^2} - V^2)/R$, where R is the gas constant for the species. The preserved density, ρ_{IP} is usually treated on a cell basis. Macroscopic quantities are obtained by averaging the IP quantities of the simulated molecules within each cell.

As in Ref. [22], Maxwell's equation of change may be used to evaluate the transport of IP quantities as shown:

$$\frac{\partial(nm)}{\partial t} + \nabla \cdot (nm\overline{V}) = 0, \tag{1}$$

$$\frac{\partial(nm\overline{\mathbf{V}})}{\partial t} + \nabla \cdot (nm\overline{\mathbf{c}\mathbf{V}}) = -\nabla \cdot (nm\overline{\mathbf{c}'\mathbf{c}'''}), \tag{2}$$

$$\frac{\partial}{\partial t}(nm(\overline{V^2 + 3RT_{\mathrm{IP}}})) + \nabla \cdot (nm\overline{\mathbf{c}(V^2 + 3RT_{\mathrm{IP}})}) = -\nabla \cdot (nm\overline{\mathbf{c}'(V^2 + 3RT_{\mathrm{IP}} - c^2)}), \tag{3}$$

where n is the number density, m is the molecular mass, $\mathbf{c}' = \mathbf{c} - \mathbf{c}_0$ is the peculiar velocity, $c_0 = \bar{c} = \overline{\mathbf{V}}$ is the stream velocity, and $\mathbf{c}''' = \mathbf{c} - \mathbf{V}$. The second terms on the left-hand side of Eqs. (2) and (3) are convective terms, corresponding to the changes in the IP quantities due to microscopic movement of simulation molecules. The right-hand side in Eq. (2), contains the so-called momentum "correlation coefficient" from Ref.

[22], and acts as a force resulting from the gradient of the stress tensor. In the case of uniform flow (i.e., $\mathbf{V} = \mathbf{c}_0$ for each simulation molecule), it is easy to show that this term is equal to $\nabla \cdot \overline{\overline{\sigma}}$. For this reason this term may be referred to within this paper as the "pseudo force" and $nm\overline{\mathbf{c}'\mathbf{c}'''}$ as the "pseudo stress tensor." Similarly, the right-hand side in Eq. (3), $nm\mathbf{c}'(V^2 + 3RT_{\mathrm{IP}} - c^2)$, acts as a heat flux and may be referred to as the "pseudo heat flux."

Notice that the form of the pseudo stress ($\overline{\mathbf{c}'\mathbf{c}'''}$) differs from that proposed by Sun and Boyd ($\overline{\mathbf{c}'''\mathbf{c}'}$) in Ref. [22]. The familiar stress tensor, $\sigma_{ij} = \overline{c_i' c_j'}$, may be interpreted as the transport of the jth component of specific momentum in the ith direction. The preserved pseudo stress must be consistent with this interpretation, i.e., $c_i V_j$ is the transport of the jth component of preserved specific momentum (V_j) transported in the ith direction by the underlying DSMC velocity (c_i). Thus, Eqs. (1)–(3) describe the evolution of the preserved quantities as a result of particle movement and the pseudo force and pseudo heat flux acting on the cell.

An additional benefit of this corrected formulation is that it is now possible to derive workable formulae for the IP viscous stress and heat flux in terms of mixed samples of the correlation coefficients and the microscopic (DSMC) quantities of the ensemble of simulation molecules within a given computational cell:

$$\sigma_{ij} = \rho\overline{c_i V_j} + \rho\overline{c_i' c_j'''} - \rho c_{0i} c_{0j}, \tag{4}$$

$$q_i = \frac{\rho}{2}\left[\overline{(c_i(V^2 + 3RT_{\mathrm{IP}})} - \overline{c_i'(V^2 + 3RT_{\mathrm{IP}} - c^2))} - c_{0i}\overline{(V^2 + 3RT_{\mathrm{IP}})}\right] - \sigma_{ij} c_{0j}, \tag{5}$$

where $\overline{c_i V_j}$ and $\overline{c_i(V^2 + 3RT_{\mathrm{IP}})}$ are mixed terms, (i.e., sampling combinations of DSMC and information preserving quantities), $\overline{c_i' c_j'''}$ and $\overline{c_i'(V^2 + 3RT_{\mathrm{IP}} - c^2)}$ are the correlation coefficients, and $\mathbf{c}_0$ may be replaced by $\overline{\mathbf{V}}$. These formulae may be used in place of less efficient methods which sample only those particles which cross cell boundaries within a given timestep [20].

Two components are still required: a model for intermolecular interactions that distributes mass, momentum, and energy appropriately between collision partners in a conservative manner; and a means of evaluating the pseudo stress and pseudo heat flux in terms of the available information. While the collision model deserves further study, the phenomenological collision model proposed by Sun and Boyd has been shown to perform quite well [20,22] and will be used in this study.

Sun and Boyd showed that the correlation coefficients can be expressed in terms of moments of velocity distribution functions and proposed two distribution models for these: the local thermal equilibrium (LTE) and flux splitting (FS) [22]. The LTE model assumes that the velocity distribution function of each particle follows a Maxwellian, or equilibrium, distribution. The FS approach splits the particles into classes depending on their microscopic (DSMC) velocities and evaluates the correlation coefficients by taking moments of the half-Maxwellian distributions that are assumed to describe the velocity spaces of each of the associated splitting classes. The results of thermal Couette flow simulations led Sun and Boyd to determine that the Flux Splitting model was the superior method and subsequent simulations for shock structures in argon used only the FS model [22]. They also note that their previous "additional energy" method is a special case of the FS model. Later in this paper we will show that the LTE and FS methods are closely related and that the success of a correlation coefficient model depends on its ability to capture the directional non-equilibrium—or modality—of the velocity distributions.

3. Thermal transpiration

A brief explanation of the mechanism producing thermal transpiration, as well as thermal creep and the radiometric effect, will be presented here, as it is pertinent to subsequent derivations. Consider a system wherein two volumes of gas are maintained at the same initial pressure but dissimilar temperatures and joined by a tube of some length. If the width of the tube is large in comparison to the mean free path of the gas (small Kn) then the gas will diffuse through the tube preserving a uniform pressure but establishing a thermal gradient within the tube. If the tube is narrow, such that the Knudsen number is significant, then molecules will "creep" through the tube from the cold to the hot reservoir. If the reservoirs are sealed, the result will be a static pressure gradient, if they are open then the result will be a continuous transport—or pumping—from the cold to the hot reservoir.

The "creep" mechanism may be explained as follows. Molecules encountering the walls of the tube impart momentum to the wall in normal and tangential directions. Perfectly elastic collisions with a smooth wall would result in the molecule leaving the wall with the same tangential momentum but with reversed normal momentum. Such collisions are very unlikely in real systems and the post-collision momentum of the molecule is largely a function of the temperature of the wall—conforming to some thermal velocity distribution. The average tangential momentum of particles leaving the wall from a given point is zero while the molecules arriving from "hot" regions will tend to have higher velocities than molecules arriving from "colder" regions. The result is a shear force acting on the wall due to the greater momentum imparted by "hot" molecules than by "cold" ones and a reaction shear stress acting on the gas oriented toward the "hot" region. This produces a creep flow near the wall in the direction of the thermal gradient, transporting gas from cold to hot. In the transition regime, the creep flow may eventually be balanced by reverse Poiseuille flow driven by the induced pressure gradient.

As previously mentioned, many experimental observations of thermal transpiration have been reported [24,25] as well as practical application of the effect in Knudsen pumps and micropropulsion systems [4–7,24]. From a modeling standpoint, a number of different techniques have been proposed, including various solutions of the linearized Boltzmann transport equation (BGK, S-model, etc.) [26,27], near continuum slip models [10,28], and DSMC simulations [6]. Linearized BTE methods are suitable for problems with small thermal gradients, i.e., weakly non-equilibrium, but are likely inadequate for the complex geometries and large thermal gradients that may be encountered in micro- and nanoscale systems. Near continuum models are only applicable for a small range of flow conditions. With this in mind, we want to simulate strongly non-equilibrium thermally driven systems with the IP-DSMC—leveraging the flexibility of the DSMC while avoiding the computational expense usually associated with low-speed flows.

3.1. Flux splitting flow simulation of thermal transpiration

The problem we will consider in this work is a sealed 2D microchannel with a rectangular cross section and geometry suitable for MEMS applications as shown in Fig. 1. It should be noted that although we consider 2D problems in this paper, the techniques presented here are equally applicable to 3D simulations. The two ends of the channel are maintained at two different temperatures $T_1 < T_2$ ($T_1 = 273$ K and $T_2 = 573$ K). The temperature of the side walls varies linearly along the length of the channel and the working gas (Argon) is initially in thermal equilibrium with the walls (i.e., $T(x,y) = (T_2 - T_1)x/L + T_1$) and at a uniform pressure of one atmosphere, i.e., $P(x,y) = P = 1$ atm. The walls are modeled as fully accommodating and the out-of-plane height (H) is assumed be much larger than the width (W), allowing the simplification to two dimensions. This reduces the problem size to one that may be performed using a desktop workstation. The channel is discretized using 200 cells along the length and 40 along the width with an average of 100 particles per cell.

3.2. Failure of flux splitting model

Fig. 2 presents the pressure distributions along the length of the microchannel as modeled by the DSMC and the flux splitting IP-DSMC. While the DSMC solution predicts a static pressure gradient ($P_1 = 100.110$ kPa, and $P_2 = 103.688$ kPa) as expected, the FSIP-DSMC results are quite disappointing, with little change from the initial pressure distribution. Furthermore, the velocity field predicted by the DSMC begins to exhibit the anticipated recirculatory flow, with creep flow moving from cold to hot along the boundaries and a central pressure driven flow in the opposite direction (see Fig. 10). The flux splitting IP-DSMC velocity field (not shown) is essentially stationary.

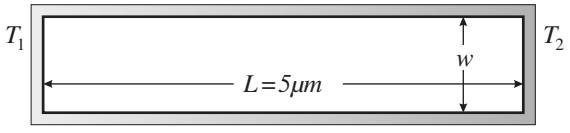

Fig. 1. Diagram of 2D thermal transpiration microchannel. Channel widths (w) used in this study are 1 μm, 100 nm, and 20 nm.

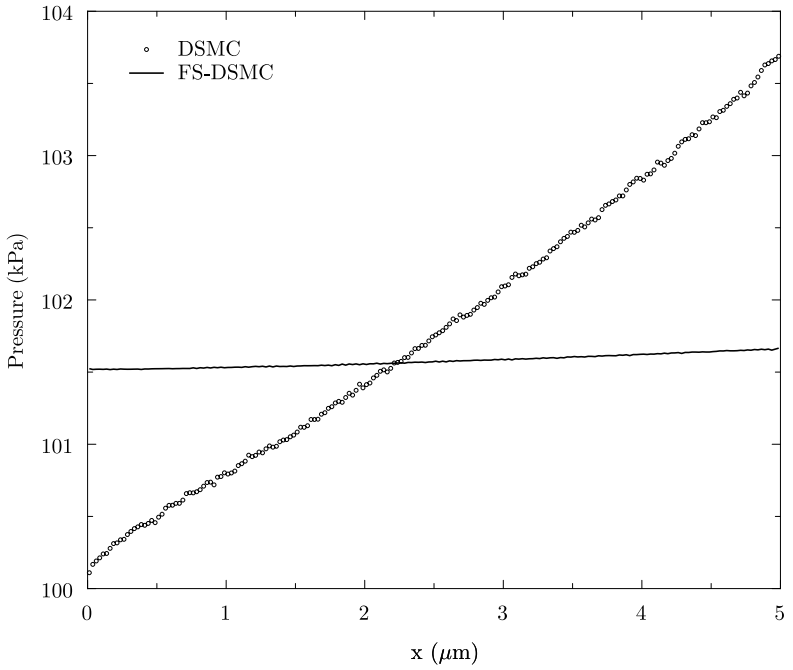

Fig. 2. Comparison of flux splitting and DSMC pressure distribution results for 5 μm × 1 μm thermal transpiration microchannel.

To understand the inability of the flux splitting IP-DSMC to correctly model thermal transpiration—and hopefully identify a correction—we must look closely at the pseudo stress tensor. In the FS approach, the pseudo stress tensor, $\overline{\mathbf{c}'\mathbf{c}''}$, of a particle is evaluated by integrating the Maxwell–Boltzmann distribution over the half-space determined by the splitting direction [22]:

$$\overline{c_k' c_j''} = \frac{\beta^3}{\pi^{3/2}} \int\int\int_{c_i \diamondsuit a_i} (c_k - c_{0k})(c_j - V_j) \mathrm{e}^{-\beta^2(\mathbf{c}-\mathbf{V})^2} \, \mathrm{d}\mathbf{c} = \begin{cases} \frac{\left(1 \overset{K}{\pm} \operatorname{erf}(\beta(V_k - a_k))\right)}{4\beta^2} \overset{K}{\mp} \frac{(c_{0j} - a_j)\mathrm{e}^{-\beta^2(V_k - a_k)^2}}{2\sqrt{\pi}\beta}, & j = k \\ 0, & j \neq k \end{cases} \tag{6}$$

where the splitting direction and the limits of integration are determined by comparing the DSMC velocity $\mathbf{c}$ for this particle to some splitting velocity, $\mathbf{a}$, such that the limits of integration are defined for each ith dimension of the integrals in Eq. (6) as

$$c_i \diamondsuit a_i = \begin{cases} -\infty \to \infty, & i \neq k, \\ \begin{cases} a_i \to \infty, & c_i > a_i \\ -\infty \to a_i, & c_i < a_i \end{cases} & i = k. \end{cases} \tag{7}$$

The terms $\overset{K}{\pm}$ and $\overset{K}{\mp}$ indicate sign (or operator) changes based on the splitting in the kth direction ($c_k > a_k$ or $c_k < a_k$, respectively). $\beta = (2RT)^{-1/2}$ is the inverse of the most probable speed. The pseudo stress terms, $\overline{\mathbf{c}'\mathbf{c}''}$, for each splitting direction are averaged over the particles in each splitting class and added together to construct the complete tensor. As may be seen from Eq. (6), the pseudo stress tensor, $\overline{\mathbf{c}'\mathbf{c}''}$, obtained from the flux splitting method, is a strictly diagonal tensor—with the "pressure" terms along the diagonal. When used in the update step, it results in a purely pressure driven flow. In the thermal transpiration problem, the net shear stress, i.e., the net transport of tangential momentum, in the real gas is nonzero in regions adjacent to the wall as a result of the temperature modality existing in the gas molecules. As previously discussed, this shear stress drives the creep flow. It is apparent from this numerical experiment and the preceding analysis that the flux splitting method has no mechanism for recovering the effect of temperature modality on shear transport and is thus incapable of modeling thermal transpiration.

4. Octant splitting method

In a non-equilibrium system, the velocity distribution of particles in a local region (or computational cell) is asymmetric. The FS approach considers certain directional biases in the velocity distribution function of the cell by using half fluxes, i.e., distinguishing in-flow and out-flow of momentum and energy with respect to the coordinate directions. However, the FS method only splits along the direction of momentum transport when calculating the components of the correlation coefficients in that direction. In the directions perpendicular to the splitting direction, the velocity distribution function used to evaluate the correlation coefficients is assumed to be symmetric (i.e., the limits of integration are $-\infty \to \infty$). As such, no shear can ever be produced. Considering the need to preserve the direction dependent non-equilibrium for all components of the pseudo stress, it seems logical to split the particles into more classes. Thus for a problem of N dimensions there will be 2^N splitting directions: two half spaces in 1D, four quadrants in 2D and eight octants in 3D. Although we are currently considering a 2D system, the following derivation is for the general 3D case. Thus for the octant method, each simulation molecule is classified as belonging to one—and only one—octant based on its microscopic DSMC velocity relative to some splitting velocity $\mathbf{a}$ (in practice the stream velocity for the cell $\mathbf{a} = \mathbf{c}_0 \approx \overline{\mathbf{V}}$ is used). As in the flux splitting method, the Maxwellian distribution function is used as the basis for the split distribution function assumed for each simulation molecule, but the limits of integration reflect the new splitting scheme. Specifically, the limits in the kth dimension are dependent on the splitting direction for the kth velocity component, i.e.,

$$S_k = \begin{cases} a_k \to \infty & \text{if } c_k > a_k, \\ -\infty \to a_k & \text{otherwise,} \end{cases} \tag{8}$$

yielding the following integration

$$\overline{c_k' c_j'''} = \frac{\beta^3}{\pi^{3/2}} \int_{S_{k-}}^{S_{k+}} \int_{S_{j-}}^{S_{j+}} \int_{S_{i-}}^{S_{i+}} (c_k - c_{0k})(c_j - V_j) \mathrm{e}^{-\beta^2(\mathbf{c}-\mathbf{V})^2} d\mathbf{c}, \tag{9}$$

where S_{k-} and S_{k+}, etc. represent the upper and lower bounds of S_k, etc. defined in Eq. (8) and the argument of the exponential, $-\beta^2(\mathbf{c} - \mathbf{V})^2$, retains the matrix notation for brevity. Integrating Eq. (9) (and exchanging indices i and k), yields:

$$\overline{c_i' c_i'''} = \left(1 \overset{J}{\pm} \operatorname{erf}(\beta(V_j - a_j))\right)\left(1 \overset{K}{\pm} \operatorname{erf}(\beta(V_k - a_k))\right)\left[\frac{RT\left(1 \overset{I}{\pm} \operatorname{erf}(\beta(V_i - a_i))\right)}{8} \overset{I}{\pm} \frac{(a_i - c_{0i})\mathrm{e}^{-\beta^2(V_i - a_i)^2}}{8\sqrt{\pi}\beta}\right], \tag{10}$$

$$\overline{c_i' c_j'''}\big|_{i \neq j} = \left(\overset{J}{\pm}\right) \frac{\mathrm{e}^{-\beta^2(V_j - a_j)^2}}{8\sqrt{\pi}\beta}\left(1 \overset{K}{\pm} \operatorname{erf}(\beta(V_k - a_k))\right)\left[(V_i - c_{0i})\left(1 \overset{I}{\pm} \operatorname{erf}(\beta(V_i - a_i))\right) \overset{I}{\pm} \frac{\mathrm{e}^{-\beta(V_i - a_i)^2}}{\sqrt{\pi}\beta}\right]. \tag{11}$$

The diagonal component, $\overline{c_i' c_i'''}$, is similar to that of the flux splitting method (differing by a factor of 1/4 and the leading terms involving the error function). However, the significant difference is that the new splitting scheme has introduced non-zero off-diagonal, or shear, components. Note that the second term within the square brackets in Eq. (10) vanishes if, as previously discussed, the stream velocity is used for the splitting velocity.

By similar means, the pseudo heat flux can be derived:

$$\overline{c_i'(V^2 + 3RT - c^2)} = E_{ii} + E_{ij} + E_{ik} \tag{12}$$

$$E_{ii} = \left(1 \overset{J}{\pm} \operatorname{erf}(\beta(V_j - a_j))\right)\left(1 \overset{K}{\pm} \operatorname{erf}(\beta(V_k - a_k))\right)\left[-\frac{V_i RT\left(1 \overset{I}{\pm} \operatorname{erf}(\beta(V_i - a_i))\right)}{4} \overset{I}{\pm} \frac{\mathrm{e}^{-\beta^2(V_i - a_i)^2}}{8\sqrt{\pi}\beta}[(c_{0i} - a_i)(V_i + a_i) - \mathrm{R}T]\right], \tag{13}$$

$$E_{ij} = \left(\overset{J}{\pm}\right)(V_j + a_j)\frac{e^{-\beta^2(V_j-a_j)^2}}{8\sqrt{\pi}\beta}\left(1 \overset{K}{\pm} \operatorname{erf}(\beta(V_k - a_k))\right)\left[(V_i - c_{0i})\left(1 \overset{I}{\pm} \operatorname{erf}(\beta(V_i - a_i))\right) \overset{I}{\pm} \frac{e^{-\beta^2(V_i-a_i)^2}}{\sqrt{\pi}\beta}\right]$$
$$= (V_j + a_j)\overline{c_i' c_j'''}, \tag{14}$$

$$E_{ik} = \left(\overset{K}{\pm}\right)(V_k + a_k)\left(1 \overset{J}{\pm} \operatorname{erf}(\beta(V_j - a_j))\right)\frac{e^{-\beta^2(V_k-a_k)^2}}{8\sqrt{\pi}\beta}\left[(V_i - c_{0i})\left(1 \overset{I}{\pm} \operatorname{erf}(\beta(V_i - a_i))\right) \overset{I}{\pm} \frac{e^{-\beta^2(V_i-a_i)^2}}{\sqrt{\pi}\beta}\right]$$
$$= (V_k + a_k)\overline{c_i' c_k'''}. \tag{15}$$

Eq. (13) will also be simplified by using the stream velocity for the splitting velocity, eliminating the product $(c_{0i} - a_i)(V_i + a_i)$. Degenerate forms of Eqs. (10)–(15) are easily developed for lower dimensions. For example, if 2D simulations are desired then the terms involving $\left(1 \overset{Z}{\pm} \operatorname{erf}(\beta(V_z - a_z))\right)$ are replaced by the constant 2 and exponential terms arising from the z-dimension vanish, e.g., $\exp(-\beta^2(V_z - a_z)^2) = 0$, this degenerate form may be called the Quadrant Method. For 1D simulations, the same arguments lead to the recovery of the flux splitting method of Sun and Boyd [22]. Finally, the zero-dimensional form recovers the local thermal equilibrium method also presented in [22]. That the LTE is a zero-dimensional form of the general octant method provides additional insight into the poor performance of the LTE.

Consider now an initially stationary two-dimensional gas bounded on the lower side by a surface whose temperature varies linearly, with T_w increasing in the positive x-direction. Furthermore, we assume that the gas is in thermal equilibrium with the boundary, such that the same temperature gradient is present in the gas. As the gas is assumed to be stationary, one may assume that the preserved velocities of all particles are also zero, however, some thermal modality exists due to the temperature gradient: particles arriving from different locations will have different temperatures. We now construct the $\overline{\mathbf{c}'\mathbf{c}'''}$ tensor as

$$\overline{\mathbf{c}'\mathbf{c}'''} = \begin{bmatrix} R\overline{T}/4 & -R\overline{T}/2\pi & 0 \\ -R\overline{T}/2\pi & R\overline{T}/4 & 0 \\ 0 & 0 & R\overline{T}/4 \end{bmatrix}_{\mathrm{NW}} + \begin{bmatrix} R\overline{T}/4 & R\overline{T}/2\pi & 0 \\ R\overline{T}/2\pi & R\overline{T}/4 & 0 \\ 0 & 0 & R\overline{T}/4 \end{bmatrix}_{\mathrm{NE}} + \begin{bmatrix} R\overline{T}/4 & R\overline{T}/2\pi & 0 \\ R\overline{T}/2\pi & R\overline{T}/4 & 0 \\ 0 & 0 & R\overline{T}/4 \end{bmatrix}_{\mathrm{SW}}$$
$$+ \begin{bmatrix} R\overline{T}/4 & -R\overline{T}/2\pi & 0 \\ -R\overline{T}/2\pi & R\overline{T}/4 & 0 \\ 0 & 0 & R\overline{T}/4 \end{bmatrix}_{\mathrm{SE}} \tag{16}$$

where the subscripts NW, NE, SW, and SE indicate the four splitting directions as compass directions, and $\overline{T}$ indicates the average IP temperature of the molecules in each splitting direction. Near the surface, molecules moving in the NW and NE directions are likely to have recently encountered the surface and will have approximately the same preserved temperature (see Fig. 3). As such, the shear terms from these classes (NW and NE) cancel $(-R\overline{T}_{\mathrm{NE}}/2\pi + R\overline{T}_{\mathrm{NE}}/2\pi = 0)$. However, particles moving SW (coming from a higher temperature region) will tend to have higher temperatures than those moving SE, resulting in net shear components

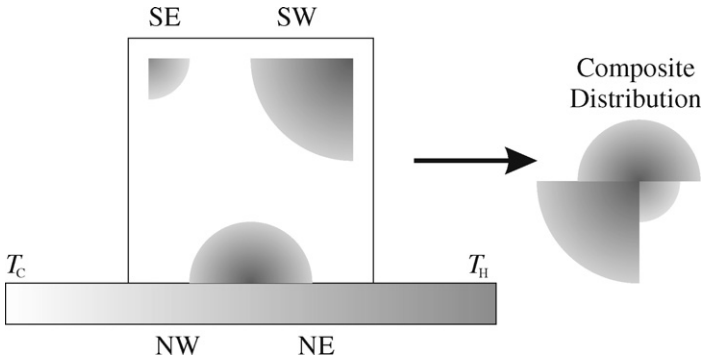

Fig. 3. Conceptual diagram of quadrant method within a computational cell near a boundary. Particles are separated into four quadrants: NE, NW, SE, SW over which the correlation coefficients are evaluated and summed to form the composite distribution.

$R(\overline{T}_{SW} - \overline{T}_{SE})/2\pi$ (see Fig. 3). Thus, the octant splitting method provides a mechanism for recovering shear components of momentum from the preserved thermal energy, even in a stationary gas. The stationary flow assumption allows Eqs. (7) and (8) to be simplified as Eq. (16) but the identical simplified result is obtained for non-stationary flow if the stream velocity is uniformly preserved, i.e., $\mathbf{V}_i = \mathbf{c}_0$. In practice, the general forms of Eqs. (7) and (8) are used to calculate the pseudo stress terms for uniform and non-uniform flow fields and will naturally degenerate in the presence of symmetric flows —automatically accounting not only for uniformity, but also degenerate forms arising from any natural symmetries.

Up to this point it would seem that the global coordinate system may be used to determine splitting classes and evaluate the fluxal terms. For the current problem, this assumption would be adequate, as one of the global coordinates coincides with the thermal gradient. For general thermally driven problems, the splitting directions should be chosen such that one of the coordinate directions is oriented in the direction of the local thermal gradient. This will facilitate capturing the effect of the thermal modality on the momentum. A choice that approximates this and is more generally applicable is to use the sampled heat flux vector. This provides the first of the direction cosines. In 2D, the projection of the heat flux vector on the x–y plane should be used as the first direction cosine and the second may be selected normal to the first. In 3D the choice of the second and third directions seems arbitrary provided that they are mutually orthogonal to the first direction cosine, but further study is needed to verify this assumption. We may now summarize the steps of the Octant flux splitting method:

1. Determine the local coordinate system from the local heat flux vector, **q** and construct the transformation matrix, **R** composed of column vectors defining the local coordinate system.
2. Perform a coordinate transformation on the stream velocity, splitting velocity, and the individual microscopic and IP velocities (e.g., $\mathbf{c}^* = \mathbf{R}^T\mathbf{c}$).
3. Calculate the correlation coefficients $(\overline{c'_k c'''_j})^*$ and $(\overline{c'_k(V^2 + 3RT - c^2)})^*$ for each simulation molecule and average over the molecules in each splitting direction. Sum the contributions from each splitting direction to obtain the complete correlation coefficients.
4. Return the correlation coefficients to the global coordinate system,

$$\overline{c'_k c'''_j} = \mathbf{R}(\overline{c'_k c'''_j})^*\mathbf{R}^T, \tag{17}$$

$$\overline{c'_k(V^2 + 3RT - c^2)} = \mathbf{R}(\overline{c'_k(V^2 + 3RT - c^2)})^*. \tag{18}$$

5. Proceed with modification step of IP-DSMC (Eqs. (1)–(3)) and sample steps (including Eqs. (4) and (5)).

5. Results

5.1. Benchmark simulation: thermal Couette flow

Before presenting simulation results for thermal transpiration, we first benchmark the octant flux splitting method for the simple 1D thermal Couette flow problem. This consists of two stationary parallel surfaces maintained at different temperatures and bounding the working gas. We apply parameters corresponding to those used by Sun and Boyd, namely: the surfaces are maintained at 173 K and 373 K with a 1 m gap between them and the intervening space is filled with Argon at various densities, such that the $Kn = 0.01$, 0.1, 1, 10, and 100 [20,22]. The 1D computational domain is discretized with 100 cells and a total of 10,000 simulation molecules are used.

Figs. 4 and 5 present the temperature profiles and heat flux results of these analyses, comparing the IP-DSMC results with the results of the underlying DSMC simulations. From these, we can observe excellent agreement for the wide range of Knudsen numbers. There is some small discrepancy in the heat flux at high Kn that becomes apparent in the log-scale plot. This may be a consequence of the IP collision model, the parameters of which were originally developed for the ''additional energy'' model of Sun and Boyd [20]. These results do agree well with published results, of note, those from the flux splitting method reported in reference [22]. This is not surprising as the OSIP-DSMC should degenerate to the flux splitting method in 1D.

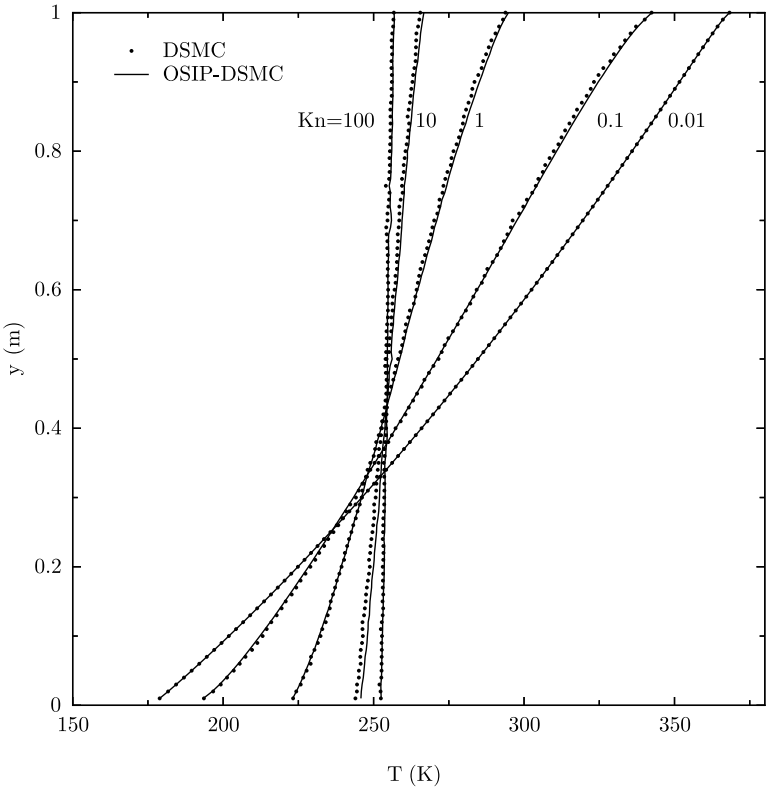

Fig. 4. Temperature profiles for thermal Couette flow for OSIP-DSMC and DSMC.

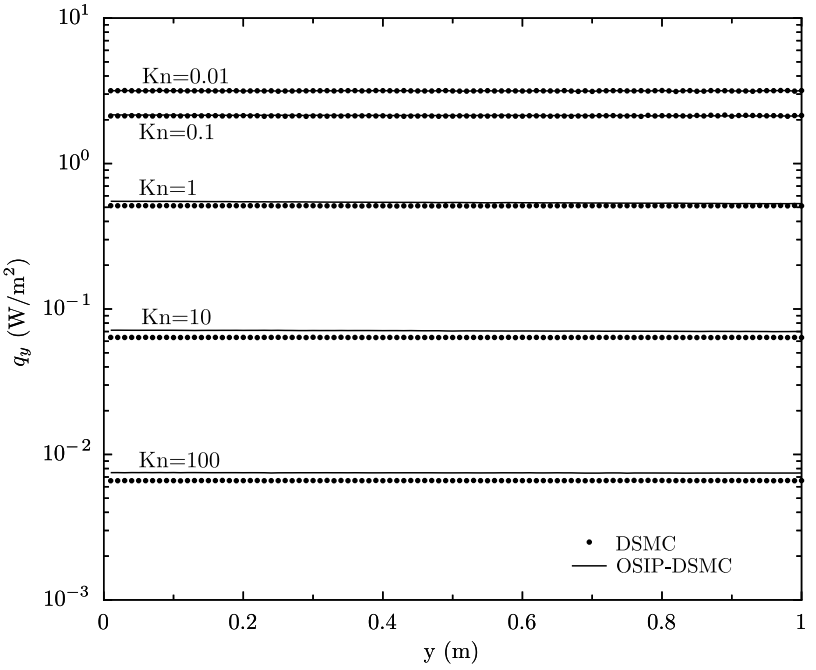

Fig. 5. Heat transfer profiles for thermal Couette flow for OSIP-DSMC and DSMC simulations of Argon at $Kn = 0.01$, 0.1, 1, 10, and 100.

5.2. OSIP-DSMC simulation of thermal transpiration

We now return to the problem of thermal transpiration using the geometry, initial and boundary conditions described previously. The IP-DSMC simulation (and underlying DSMC) where allowed to run for 60,000 timesteps prior to beginning sampling. The simulations then proceeded for and additional 288,000 timesteps accumulating 24,000 samples. The temperature profiles within the gas in both the DSMC and OSIP-DSMC simulations follow the linear temperature distribution imposed by the boundary conditions (see Figs. 6 and 7). Again, the DSMC simulation predicts a static pressure gradient as shown in Fig. 8. However, unlike the flux splitting method, the octant splitting method also predicts a static pressure gradient (see Fig. 9). The magnitudes of the OSIP-DSMC pressure gradient varies from 100.447 kPa to 103.239 kPa, which compares well with the DSMC pressure gradient of 100.110–103.688 kPa. Slight variations in the pressure distribution may be observed in both simulations near the corners of the channel.

Important features of the velocity fields are presented Figs. 10 and 11. Figs. 10a and 11a present the flow fields for the entire channel (*Note:* for clarity the number of data points has been reduced by a factor of four) for the DSMC and IP-DSMC, respectively. Figs. 10b and 11b (Figs. 10d and 11d) plot the details of the velocity field at the leftmost (or rightmost) 0.6 μm of the channel, wherein the recirculatory flow is readily apparent, as is the significant noise reduction in the OSIP-DSMC results. Figs. 10c and 11c present the distribution of the x-component of velocity as a function of transverse position averaged over the portion of the channel from

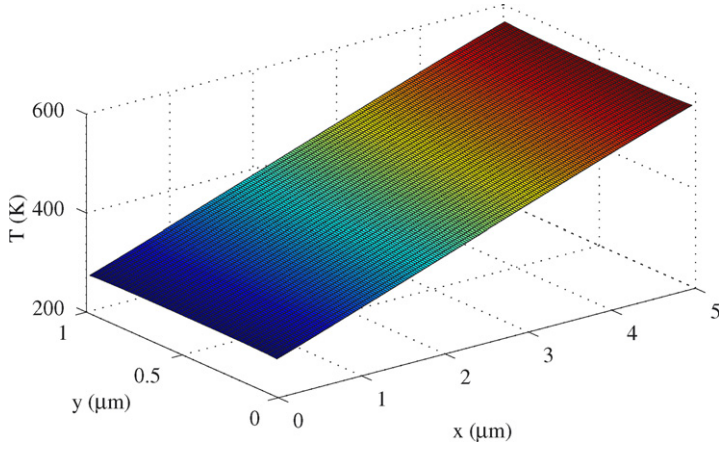

Fig. 6. DSMC temperature distribution for 5 μm × 1 μm thermal transpiration microchannel.

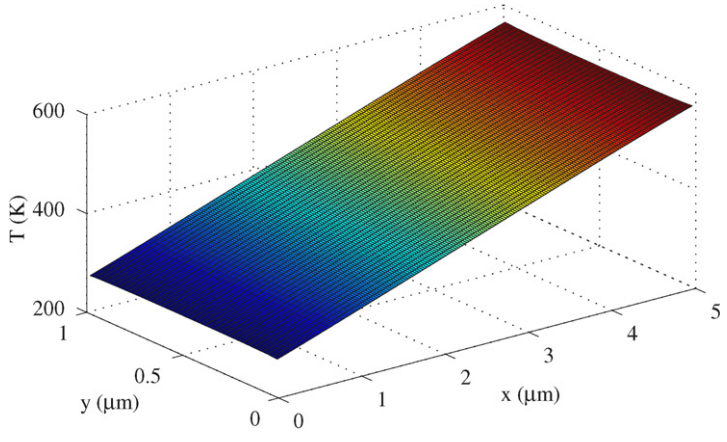

Fig. 7. OSIP-DSMC temperature distribution for 5 μm × 1 μm thermal transpiration microchannel.

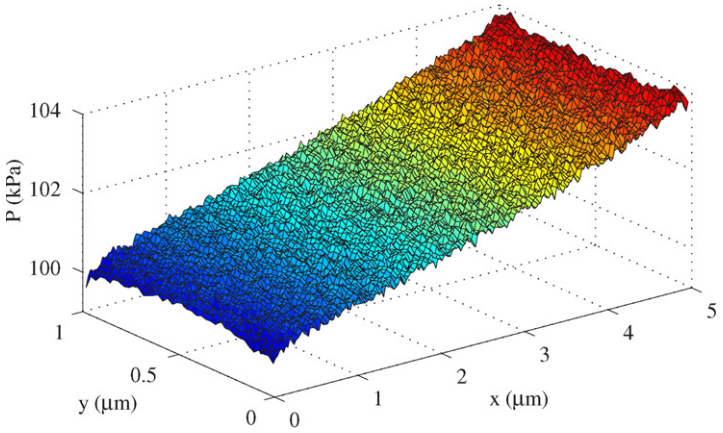

Fig. 8. DSMC pressure distribution for 5 μm × 1 μm thermal transpiration microchannel.

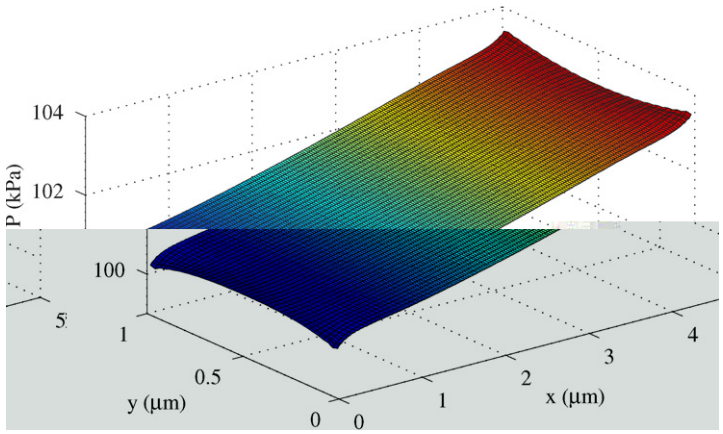

Fig. 9. OSIP-DSMC pressure distribution for 5 μm × 1 μm thermal transpiration microchannel.

1 μm to 4 μm. The error bars represent 1 standard deviation in the spatial averages $\langle \overline{V_x} \rangle$ and $\langle \overline{c_x} \rangle$, which have maximum values of 0.0049 and 0.2275 m/s, respectively. (*note:* the very small error bars in Fig. 11c are virtually obscured by the velocity profile). The DSMC would require significantly more samples to achieve the resolution obtained by the OSIP-DSMC. The maximum velocity observed in the OSIP-DSMC is 0.872 m/s and occurs near the wall.

Additional simulations were performed for thermal transpiration systems subject to the same loading, but with channel widths of 100 nm and 20 nm. The pressure profiles for these, as well as the 1 μm wide channel are presented in Table 1 and Fig. 12. As an additional point of comparison, the linearized BTE solution for the thermal transpiration problem proposed by Sharipov [26,27] is included. Considering the different modeling techniques and the obvious noise remaining in the DSMC results, the correspondence between the three models is quite good and demonstrates the ability of the OSIP-DSMC to provide detailed information of all flow characteristics at a substantially lower computational expense than the DSMC.

5.3. Simulations of flows arising from temperature discontinuities

We considered two additional problems arising from thermal loading, both dealing with temperature discontinuities on the boundary of a sealed 2-D domain. The first was described by Aoki et al. and

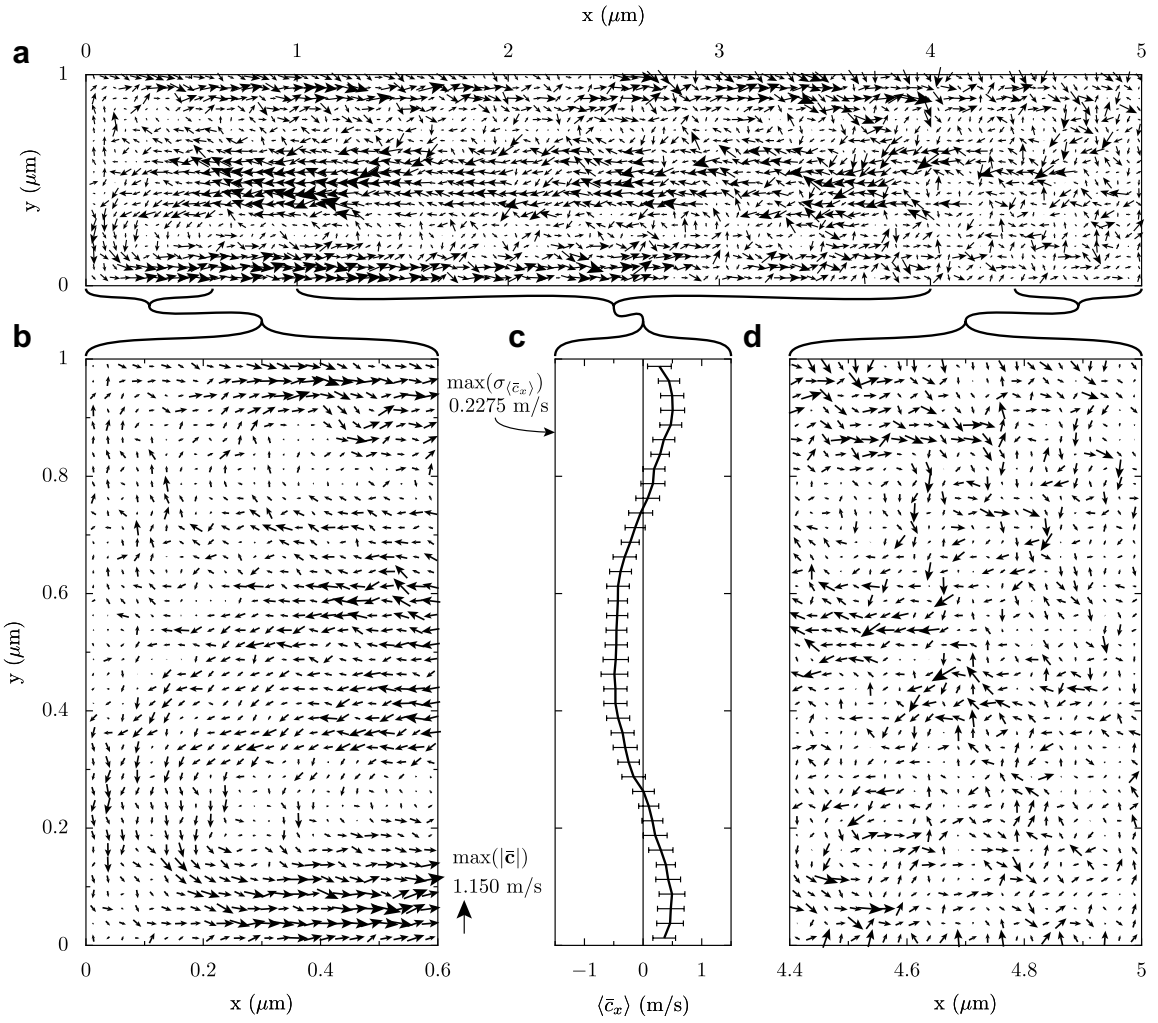

Fig. 10. Thermal transpiration: DSMC velocity distribution: (a) full channel (reduced data set); (b) leftmost 0.6 μm (full data set); (c) velocity distribution averaged over channel from 1 mm to 4 μm (error bars indicate one standard deviation); (d) rightmost 0.6 μm (full data set).

consists of a 1 μm square domain with the right and left halves of the boundary assigned different temperatures ($T_1 = 200$ K and $T_2 = 400$ K) such that temperature discontinuities are located at the midpoints of the upper and lower bounds [29] (see Fig. 13). The resulting thermal stresses in the gas drive a rotational flow, symmetric about the horizontal mid-plane of the system, as shown in Fig. 14 [29]. We applied the OSIP-DSMC to this problem: discretizing the lower half of the domain with 40 cells in the x-direction and 20 in the y-direction. The cells are initialized with an average of 100 particles per cell and an initial density such that $Kn = 0.2$. Figs. 15 and 16 present the DSMC and OSIP-DSMC velocity fields after 600,000 timesteps and a total of 40,000 samples. While the flow was fully developed and resolved in the OSIP-DSMC much sooner than this, a larger number of samples were performed to obtain the DSMC solution for comparison. In terms of both velocity distribution and magnitude, the OSIP-DSMC solution compares well with both the DSMC and the linearized BTE solution of Aoki et al. Note the velocities in these results have been normalized by the most probable velocity of the gas at T_1, i.e., $c_{mp} = \sqrt{2RT_1}$ to allow for direct comparisons with the published results of Aoki et al. The legend arrow in Fig. 14 seems to be showing an order of magnitude for the flow, whereas we chose to set the legend arrow in Figs. 15

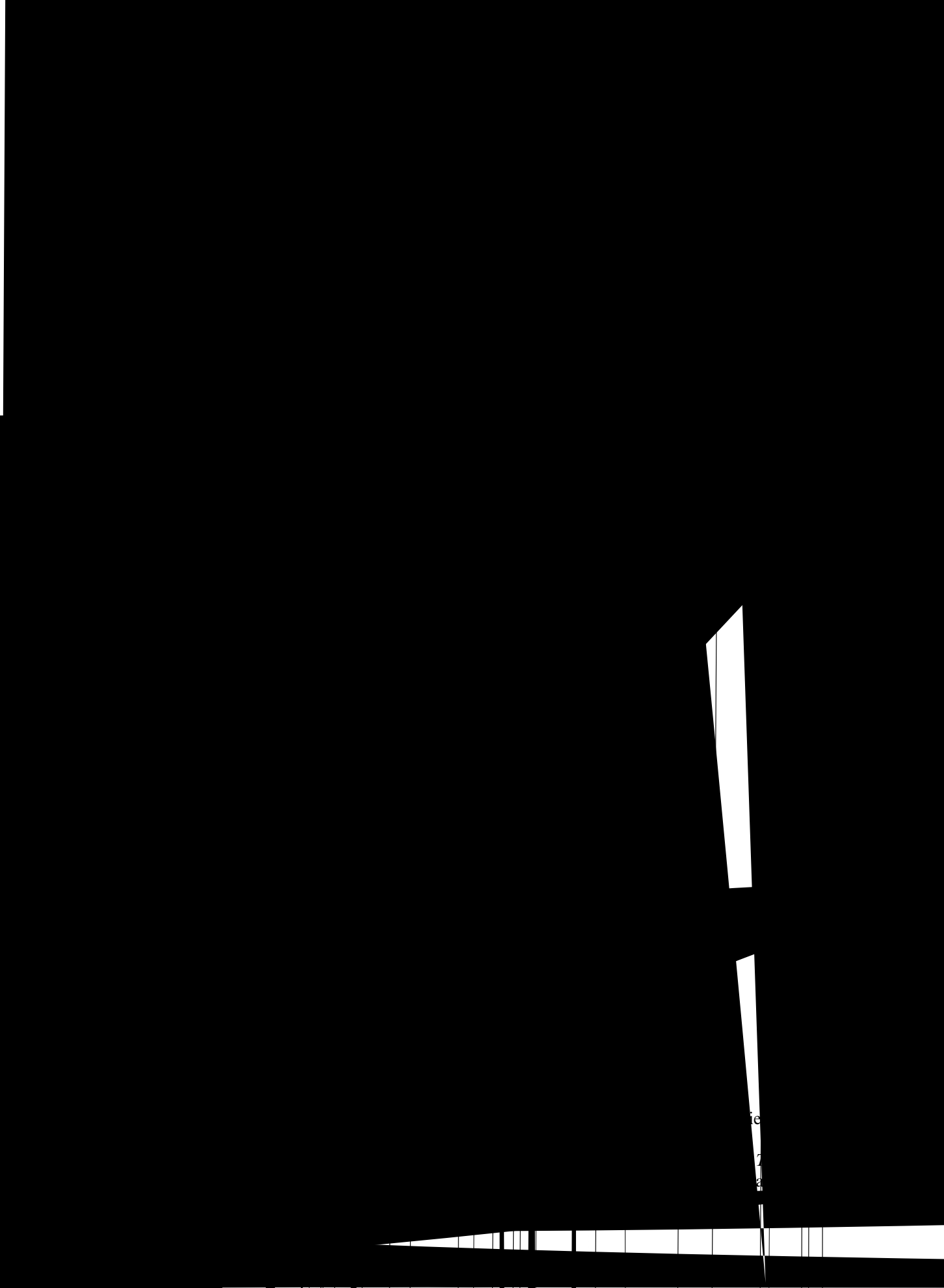

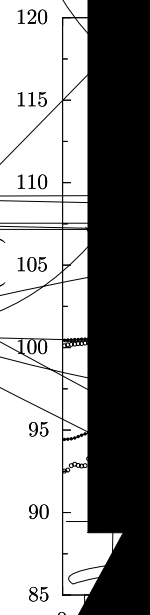

Fig. 13. Split box
is a discontinuity at the

problem but with different boundary conditions and
ing to $Kn \approx 0.1$). The results of the DSMC and OSI
respectively. The simulation was stopped after 12,0
the flow is fully resolved in the OSIP-DSMC simula
mum velocity of approximately 0.5 m/s (see Fig. 19)

6. Conclusions

Efficient techniques capable of accurately simulati
orium rarefied gas flows are needed to facil-
itate the analysis and design of a growing number
and nanoscale systems. Many such systems

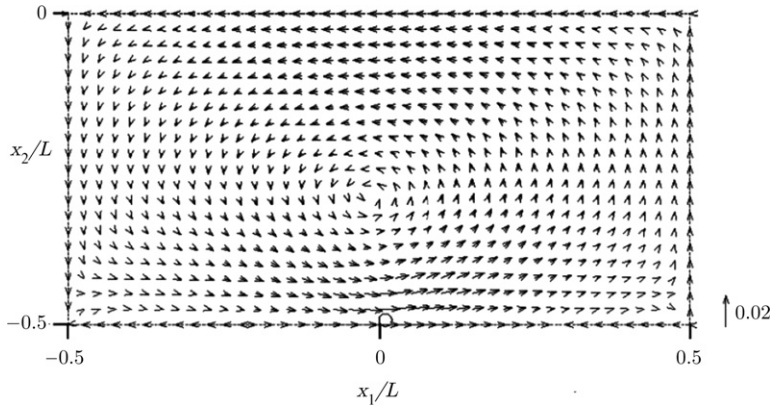

Fig. 14. Split box: velocity field (reference solution, Aoki et al. [29]).

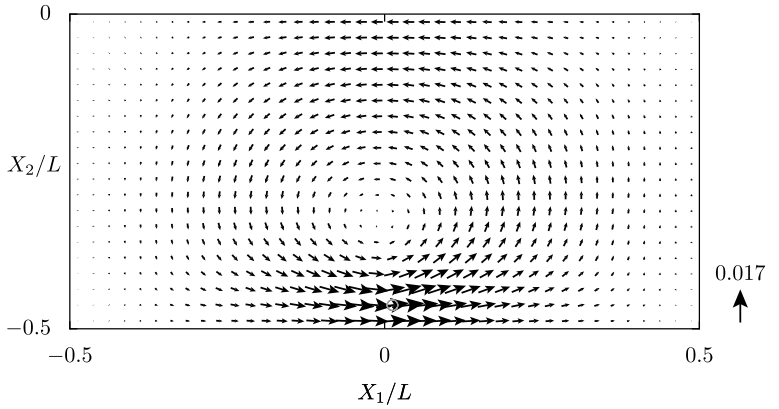

Fig. 15. Split box: OSIP-DSMC velocity field.

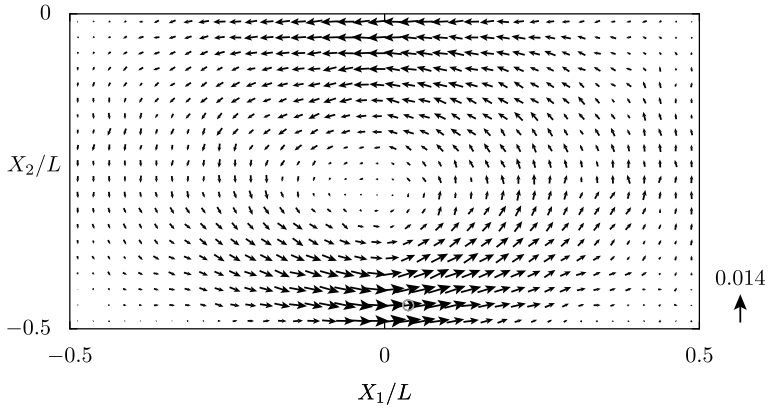

Fig. 16. Split box: DSMC velocity field.

involve low-speed flows generated by thermal gradients. Conventional DSMC simulations may be prohibitively expensive and other methods may not be satisfactory when applied to strongly non-equilibrium systems. The IP-DSMC method is an attractive solution, improving the efficiency of the DSMC while maintaining much of the flexibility and ease of implementation. However, although there have been considerable advances

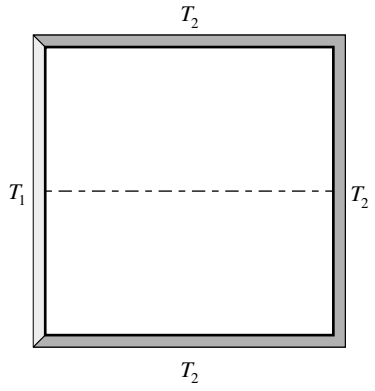

Fig. 17. Thermal cavity problem consists of a 2D sealed region 1 μm square domain with constant temperatures applied to the sides as shown. Simulation modeled lower half of the domain.

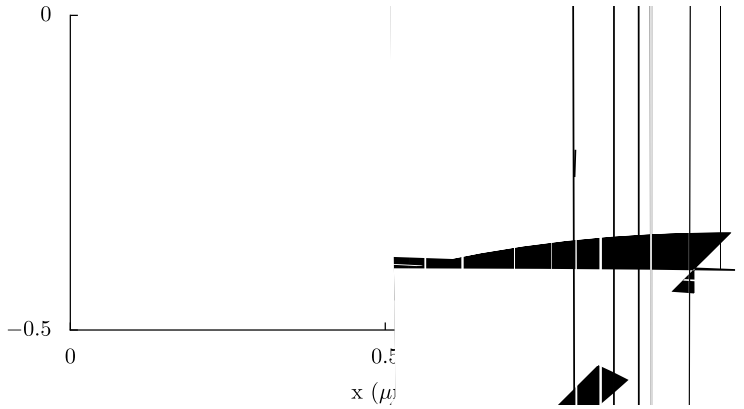

in the IP-DSMC, we have demonstrated that previous methods are unable to capture the behavior of thermal transpiration and identified the key cause, i.e., the failure to represent the asymmetric velocity distribution of the cell. By further splitting of the velocity space, the Octant Splitting IP-DSMC recaptures some of the information regarding the non-equilibrium velocity distribution that would otherwise be lost. We have also shown

that the method degenerates naturally to a quadrant splitting method in 2D and the flux splitting (1D) and local thermal equilibrium (0D) methods of Sun and Boyd. Through benchmark 1D problems and comparison with DSMC and linearized BTE solutions for a number of 2D flows, we have been able to demonstrate the ability of the OSIP-DSMC to accurately model much of the behavior arising from thermally driven non-equilibrium flows. The OSIP-DSMC provides an accurate and efficient method for a wide range of low-speed flows. Additional work is needed to validate the method for additional flows, including shock fronts, radiometer vanes, and more complex thermal loading, e.g., simulation of heated AFM cantilevers.

Acknowledgements

The authors thank the Woodruff School of Mechanical Engineering (Georgia Institute of Technology) and the National Science Foundation (Grants CCR 0306664 and EEC 0508281) for funding this work. Portions of this work were performed under the auspices of the US Department of Energy by the University of California Lawrence Livermore National Laboratory under Contract No. W-7405-ENG-48.

References

[1] E.H. Kennard, Kinetic Theory of Gases, McGraw-Hill, New York, 1938.
[2] L.B. Loeb, The Kinetic Theory of Gases, third ed., Dover Classics, New York, 1961.
[3] S. McNamara, Y.B. Gianchandani, On-chip vacuum generated by a micromachined Knudsen pump, Journal of Microelectromechanical Systems 14 (2005) 741–746.
[4] S.E. Vargo, E.P. Muntz, Initial results from the first MEMS fabricated thermal transpiration-driven vacuum pump, in: Presented at Rarefied Gas Dynamics: 22nd International Symposium, 2001.
[5] S.E. Vargo, E.P. Muntz, G.R. Shiflett, W.C. Tang, Knudsen compressor as a micro- and macroscale vacuum pump without moving parts or fluids, Journal of Vacuum Science and Technology A 7 (1999) 2308–2313.
[6] A.A. Alexeenko, S.F. Gimelshein, E.P. Muntz, A.D. Ketsdever, Modeling of thermal transpiration flows for Knudsen compressor optimization meeting, in: Presented at 43rd Aerospace Sciences Meeting, Reno, NV, AIAA Paper 2005-963, 2005.
[7] F. Ochoa, C. Eastwood, P.D. Ronney, B. Dunn, Thermal transpiration based microscale propulsion and power generation devices, in: Presented at 7th International Microgravity Combustion Workshop, Cleveland, OH, 2003.
[8] W.P. King, T.W. Kenny, K.E. Goodson, G.L.W. Cross, M. Despont, U. Durig, H. Rothuizen, G.K. Binnig, P. Vettiger, Design of atomic force microscope cantilevers for combined thermomechanical writing and reading in array operation, Journal of Microelectromechanical Systems 11 (2002) 765–774.
[9] G.A. Bird, Molecular Gas Dynamics and the Direct Simulation of Gas Flows, Clarendon Press, Oxford University Press, 1994.
[10] G.E. Karniadakis, A. Beskok, Microflows, second ed., Springer Verlag, 2001.
[11] C. Cercignani, The Boltzmann Equation and its Applications, Springer-Verlag, New York, 1988.
[12] N.G. Hadjiconstantinou, A.L. Garcia, M. Bazant, G. He, Statistical error in particle simulations of hydrodynamic phenomena, Journal of Computational Physics 187 (2003) 274–297.
[13] L.S. Pan, G.R. Liu, B.C. Khoo, B. Song, A modified direct simulation Monte Carlo method for low-speed microflows, Journal of Micromechanics and Microengineering 10 (2000) 21–27.
[14] L.S. Pan, T.Y. Ng, D. Xu, K.Y. Lam, Molecular block model direct simulation Monte Carlo method for low velocity microgas flows, Journal of Micromechanics and Microengineering 11 (2001) 181–188.
[15] J. Chun, D.L. Koch, A direct simulation Monte Carlo method for rarefied gas flows in the limit of small Mach number, Physics of Fluids 17 (2005) 107107-1–107107-14.
[16] J. Fan, C. Shen, Statistical simulation of low-speed unidirectional flows in transition regime, in: Rarefied Gas Dynamics: 21st International Symposium, Marseille, France, pp. 245–252, 1999.
[17] I.D. Boyd, Q. Sun, Particle simulation of micro-scale gas flows, in: Presented at 39th AIAA Aerospace Sciences Meeting & Exhibit, Reno, NV, 2001.
[18] J. Fan, C. Shen, Statistical simulation of low-speed rarefied gas flows, Journal of Computational Physics 167 (2001) 393–412.
[19] C. Shen, J.Z. Jiang, J. Fan, Information preservation method for the case of temperature variation, in: Rarefied Gas Dynamics: 22nd International Symposium, Sydney, Australia, pp. 185–192, 2001.
[20] Q. Sun, I.D. Boyd, A direct simulation method for subsonic microscale gas flows, Journal of Computational Physics 179 (2002) 400–425.
[21] W.-L. Wang, I.D. Boyd, A new energy flux model in the DSMC-IP method for nonequilibrium flows, in: Presented at 36th AIAA Thermophysics Conference, Orlando, FL, 2003.
[22] Q. Sun, I.D. Boyd, Theoretical development of the information preserving method for strongly nonequilibrium gas flows, in: Presented at 38th AIAA Thermophysics Conference, Toronto, Ontario, Canada, 2005.
[23] C. Cai, I.D. Boyd, J. Fan, G.V. Candler, Direct simulation methods for low-speed microchannel flows, Journal of Thermophysics and Heat Transfer 14 (2000) 368–378.
[24] B.K. Annis, Thermal creep in gases, Journal of Chemical Physics 57 (1972) 2898–2905.

[25] M. Knudsen, The Kinetic Theory of Gases, third ed., Wiley, New York, 1950.
[26] F. Sharipov, Rarefied gas flow through a long tube at any temperature ratio, Journal of Vacuum Science and Technology A 14 (1996) 2627–2635.
[27] F. Sharipov, Non-isothermal gas flow through rectangular microchannels, Journal of Micromechanics and Microengineering 9 (1999) 394–401.
[28] J.R. Bielenberg, H. Brenner, A continuum model of thermal transpiration, Journal of Fluid Mechanics 546 (2006) 1–23.
[29] K. Aoki, S. Takata, A. Hidefumi, F. Golse, A rarefied gas flow caused by a discontinuous wall temperature, Physics of Fluids 13 (2001) 2645–2661.
[30] M. Wang, Z. Li, Failure analysis of the molecular block model for the direct simulation Monte Carlo method, Physics of Fluids 16 (2004) 2122–2125.